Electrowetting: a convenient way to switchable wettability patterns

2005 J. Phys.: Condens. Matter 17 S559

(http://iopscience.iop.org/0953-8984/17/9/016)

INSTITUTE OF PHYSICS PUBLISHING JOURNAL OF PHYSICS: CONDENSED MATTER

J. Phys.: Condens. Matter **17** (2005) S559–S576 doi:10.1088/0953-8984/17/9/016

Electrowetting: a convenient way to switchable wettability patterns

F Mugele, A Klingner, J Buehrle, D Steinhauser and S Herminghaus

Department of Applied Physics, University of Ulm, Albert-Einstein-Allee 11, D-89081 Ulm, Germany

Received 24 November 2004
Published 18 February 2005
Online at stacks.iop.org/JPhysCM/17/S559

Abstract

Electrowetting is a versatile tool to reduce the apparent contact angle of partially wetting conductive liquids by several tens of degrees via an externally applied voltage. We studied various fundamental and applied aspects of equilibrium liquid surface morphologies both theoretically and experimentally. Our theoretical analysis showed that surface profiles on homogeneous surfaces display a diverging curvature in the vicinity of the three phase contact line. The asymptotic contact angle at the contact line is equal to Young's angle, independent of the applied voltage. With respect to the morphology of the liquid surface, contact angle variations achieved by electrowetting are equivalent to those achieved by varying the chemical nature of the substrates, except for electric field-induced distortions in a region close to the contact line. Experimentally, we studied the (global) morphology of liquid microstructure substrates with stripe-shaped electrodes. As the local contact angle is reduced by increasing the applied voltage, liquid droplets elongate along the stripe axis as expected. For droplets on a single surface with a stripe electrode, there is a discontinuous morphological transition where elongated droplets transform into translationally invariant cylinder segments with the contact line pinned along the stripe edge and vice versa. If the liquid is confined between two parallel surfaces with parallel stripe electrodes, the elongation of the droplet and its transformation into a translationally invariant morphology with pinned contact lines is continuous. Experimental results are compared to analytical and numerical models.

(Some figures in this article are in colour only in the electronic version)

Wetting of complex surfaces has attracted much attention in the last decade [1–4]. It became clear that both surface topography as well as lateral chemical patterns can give rise to various desirable surface properties, such as super-hydrophilicity or super-hydrophobicity, with many applications both in nature and in technology. For instance, hydrophilic stripes

in the vicinity of hydrophobic stripes may work as extremely efficient sinks in vapour condensation. More generally, chemical gradients can give rise to efficient transport of adsorbed liquid droplets. The advent of self-assembled monolayers [5] and micro-contact printing [6] enhanced the possibilities of manufacturing surfaces with specifically tailored surface chemistry tremendously. Complex fluid microstructures can now be generated and studied in detail. It turned out that the combination of complex wettability patterns and free liquid–vapour interfaces gives rise to a wealth of different morphologies and sometimes to unexpected symmetry-breaking morphological transitions [2]. A detailed analysis of liquid surface profiles on patterned surfaces, which was pushed down from the micrometre to the nanometre scale using atomic force microscopy [7], also helped to clarify long-standing debates on fundamental issues of wetting science such as line tension [8]. To a large extent the success of this program relied on the combination of careful experiments with often quantitative theoretical and numerical work [2, 9].

The surface properties in these initial studies were static. The surfaces may promote liquid transport owing to their specific design; however, no elements were included to control transport actively. More recently, with the advent of biotechnology, the desire to manipulate liquids on the micrometre scale became stronger. Most approaches involve miniaturized channels, valves, switches, etc, embedded into a solid matrix [10]. In the context of wetting, the goal is to manipulate tiny droplets with free liquid–vapour or liquid–liquid interfaces. Various strategies were explored to gain active control on fluid behaviour by tuning interfacial energies. One possibility is to create gradients of the liquid–vapour interfacial tension, which then give rise to surface-driven flow, known as the Marangoni effect. Such gradients occur in the presence of gradients in the chemical composition of the liquid as in the famous example of tears of wine (or liquor) or in the presence of temperature gradients [3, 11]. Alternatively, it is also possible to switch the properties of the substrate surface. For instance, this can be achieved chemically by altering the conformation of molecules at the surface. Self-assembled monolayers of specific molecules may be switched between different conformations which then give rise to different surface energies and contact angles. External parameters to activate the switching include UV light [12], temperature [13], or by electrochemical processes [14]. Despite the great scientific appeal of controlling macroscopic properties such as wetting and of manipulating macroscopic quantities of material by merely switching the properties of a single molecular layer, the practical use of these techniques remains to be proven. Often, the absolute variation in contact angle is rather small. Furthermore, reproducibility is often limited to a small number of switching cycles. Since the approach relies just on a single monolayer of active material, any molecule that fails affects the overall switching performance.

In contrast, electrically induced control of fluid motion is very reliable. This strategy relies on volume effects and is thus not affected by possible deterioration of individual molecules at surfaces. Despite being intrinsically body forces, electrical forces can act as if they were surface forces in suitable geometries (see figure 1(a)). In this case, the wettability can be tuned by applying a voltage between a conductive liquid and a counter-electrode [15]. In the most commonly used configuration, so-called electrowetting on a dielectric, the liquid and the counter-electrode are separated by a thin insulating layer that prevents the flow of net currents and thus the decomposition of the liquid by electrolysis. The contact angle modulation that can be achieved usually amounts to several tens of degrees, and in many cases more than 90°. The switching is perfectly reversible and was shown to last for hundreds of thousands of cycles without noticeable deterioration. There is very little power consumption because virtually only capacitive currents occur. If the counter-electrodes are patterned (typically by conventional lithographic techniques), virtually any wettability pattern that can be created by chemical surface patterning can also be realized

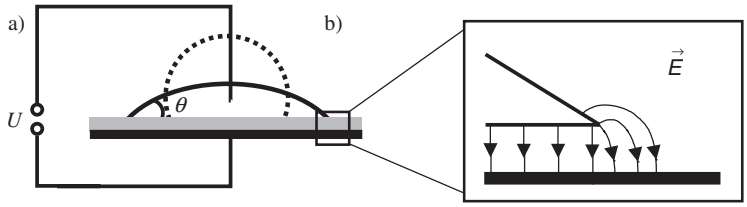

Figure 1. (a) Electrowetting setup. The counter-electrode is shown in black at the bottom. Grey: insulating layer. Droplet displays Young's contact angle at zero voltage (dashed curve) and a reduced contact angle at finite voltage (solid). (b) Magnified view of the contact line. Thin solid lines indicate the electric field distribution.

in electrowetting[1]. The advantage is, however, that the wettability contrast on the surface can be tuned continuously between zero and its maximum value. Switching rates of the wettability are extremely fast. Usually they are limited by the time constant of the power supply. Practical response times of the liquid are determined by the size-dependent mechanical resonance frequency of the droplet, which is of the order of 100 Hz for millimeter-sized droplets. This fast response time makes electrowetting attractive not only for applications in microfluidics, but also for optical applications [16], communication technology [17], and display technology [18].

In this paper, we demonstrate the use of continuously switchable wettability patterns in order to induce morphological transitions in fluid microstructures. First, we give a theoretical introduction into the concept of electrowetting and discuss some specific aspects related to non-local effects. After a brief description of experimental details, we discuss morphological transitions of liquid droplets on hydrophobic surfaces, which can be made hydrophilic locally along thin stripe electrodes. We will discuss the case of droplets on a single substrate as well as droplets confined in a gap between two parallel substrates. For the latter case, we will present a simple analytical model to describe the morphological transformation as a function of the wettability contrast.

1. Theory

The generic geometry of an electrowetting setup is shown in figure 1(a). A droplet of a partially wetting conductive liquid is deposited on a thin chemically homogeneous insulating surface, which covers a counter electrode. The free energy F is a functional of the liquid morphology. The latter is characterized by its surface A. F contains contributions from both F_{surf}, the surface energies with i (i = lv (liquid–vapour), sl (solid–liquid), sv (solid–vapour)), and from the electric field energy F_{el}.

$$F[A] = F_{\mathrm{surf}} + F_{\mathrm{el}} = \sum_i \sigma_i A_i - \int \tfrac{1}{2}\vec{E}\vec{D}\,\mathrm{d}V. \tag{1}$$

Note that the electric field energy enters with a negative sign because the battery required to sustain the potential difference is an integral part of the system [19]. At zero voltage, minimization of (1) leads to spherical cap shaped droplets with a contact angle θ_{o} that is given by Young's equation:

$$\cos\theta_{\mathrm{o}} = \frac{\sigma_{\mathrm{sv}} - \sigma_{\mathrm{sl}}}{\sigma_{\mathrm{lv}}}. \tag{2}$$

[1] The only limitation is that the minimum feature size is determined not only by the resolution of the lithographic technique, but also by the thickness of the insulator, which is often a few micrometres.

At finite voltage, the morphology of the liquid depends on the distribution of the electric field. The liquid is treated as a perfect conductor. Thus the field inside the droplet vanishes. There are two remaining contributions to the electric field energy: the first (and dominant) contribution arises from the integral over the volume of the insulating layer between the counter-electrode and the solid–liquid interface. This contribution is the same as the energy of a parallel plate capacitor with thickness d_{ins} and area A_{sl}.

$$F_1^{\mathrm{el}} = -\frac{1}{2}\frac{\varepsilon\varepsilon_0}{d_{\mathrm{ins}}}U^2 A_{\mathrm{sl}}. \tag{3}$$

Here, ε is the dielectric constant of the insulator, ε_0 is the dielectric constant of vacuum, and U is the applied voltage. The second contribution, F_2^{el}, arises from the electric stray fields in the vicinity of the contact line. For sufficiently large droplets, this contribution is negligible because it is only proportional to the length of the contact line[2], whereas F_1^{el} is proportional to A_{sl}. If we neglect F_2^{el}, (1) can be rewritten as

$$F[A] = \sigma_{\mathrm{lv}} A_{\mathrm{lv}} + \left(\sigma_{\mathrm{sl}} - \sigma_{\mathrm{sv}} - \frac{1}{2}\frac{\varepsilon\varepsilon_0}{d_{\mathrm{ins}}}U^2 \cdot \Phi_{\mathrm{el}}(\vec{r})\right) A_{\mathrm{sl}}. \tag{4}$$

Here, $\Phi_{\mathrm{el}}(\vec{r}) = 1$ when $\vec{r}$ is one on top of the electrode and zero elsewhere. If we consider a single homogeneous electrode ($\Phi_{\mathrm{el}} \equiv 1$), this equation has the same form as the one in the derivation of Young's equation, except for the electric term that gives rise to a modified prefactor for A_{sl}. Therefore, the equilibrium shape is also a spherical cap but with a different contact angle that is given by

$$\cos\theta = \cos\theta_{\mathrm{o}} + \eta. \tag{5}$$

Here, $\eta = \varepsilon\varepsilon_0 U^2/(2\sigma_{\mathrm{lv}} d_{\mathrm{ins}})$ is the dimensionless electrowetting number[3]. It measures the ratio between electrostatic energy per unit area and the surface energy σ_{lv}. The analogy between (5) and Young's equation (2) led some researchers to the statement that electrowetting changes the surface energy. This conclusion is valid for most practical purposes; however, one should keep in mind that electrical forces are in fact body forces and not surface forces. For geometric reasons they give rise to variations of the apparent contact angle in the same way as variations of the true (chemical) surface energies. However, deviations appear when we look in detail at the surface profiles close to the contact line.

Contribution of electric stray fields

As mentioned above, the contribution of F_2^{el} to the total free energy is negligible for sufficiently large droplets. Therefore, the apparent contact angle sufficiently far away from the contact line is not affected. However, F_2^{el} does affect the morphology of the liquid surface in the vicinity of the contact line. At sufficiently small scale, this region looks like a wedge (see figure 1(b)). It is clear from elementary electrostatics that the electric field in the vicinity of such a sharp edge should diverge if a voltage is applied. Since the electric field drops from a diverging value just outside the surface to zero inside the liquid, there is a diverging Maxwell stress P_{el} acting on the surface.

$$P_{\mathrm{el}}(\vec{r}) = \frac{\varepsilon_0}{2}\vec{E}(\vec{r})^2. \tag{6}$$

Here $\vec{E}(\vec{r})$ is the local electric field. In mechanical equilibrium, the mechanical stresses at a free boundary must be balanced. The only possibility for the liquid to compensate this stress

[2] Additionally, a logarithmic or a square root correction may appear (see reference [24]). In any case, the increase is weaker than for $\mathbf{F}_1^{\mathrm{el}}$.

[3] In the case of two substrates it becomes $\eta = \varepsilon\varepsilon_0 U^2/(8\sigma_{\mathrm{lv}} d_{\mathrm{ins}})$ because of $U/2$ on each substrate.

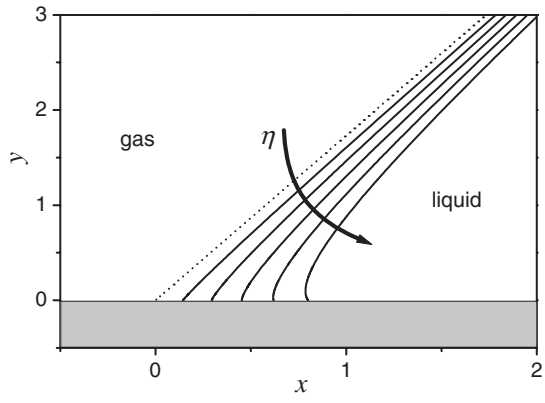

Figure 2. Drop profiles (solid curves) near to the contact line for various values of η. The dashed line is the drop profile without any potential ($\eta = 0$).

is to increase its curvature. Mechanical equilibrium can only be reached if P_{el} is balanced locally by the Laplace pressure. As $y(x)$ represents the liquid profile and y' and y'' its first and second derivatives, respectively, this gives

$$\sigma_{\mathrm{lv}} \frac{y''}{(1+y'^2)^{3/2}} = \frac{\varepsilon_0}{2} \vec{E}(\vec{r})^2. \tag{7}$$

This equation is equivalent to the condition for mechanical equilibrium in the presence of molecular forces within the so-called interface displacement model of wetting science [20]. In electrowetting, the Maxwell stress replaces the disjoining pressure, which represents the molecular forces in conventional wetting theory. The only—but crucial—difference is that the disjoining pressure can usually be assumed to be a local quantity [4], whereas the electric field and thus the Maxwell stress at $\vec{r}$ in (7) depends on the global shape of the solid–liquid interface. Therefore, the surface profile cannot be obtained by simply integrating (7) for a given field distribution, but both parts of the problem must be calculated together in a self-consistent fashion.

We performed such a calculation for a two-dimensional system, corresponding to the limit of infinite droplet radius [21]. The main results are as follows. First, the equilibrium profiles are indeed curved, as shown in figure 2. The electric field-induced distortions of the liquid surface are confined to a small region within $\approx d_{\mathrm{ins}}$ of the contact line. The curvature of the surface and thus the Maxwell stress diverges algebraically as the contact line is approached with an exponent $-1 < \mu < 0$. Nevertheless, the profiles cross the substrate surface at a finite angle. (The exact value of μ depends on this angle [21].) It turned out that this angle is equal to Young's angle θ_{o} independent of the applied voltage. Given that the apparent contact angle can be reduced by several tens of degrees, this result looks surprising at first glance. However, it is simply a manifestation of the fact that the electric forces are body forces and not true surface forces. The divergence of the electric field is too weak to give rise to a net force on the contact line [22]. For the specific case considered here, this conclusion can be verified by an analytic asymptotic expansion of the field distribution close to the contact line [21]. Another important result of the calculation is that—within this model—the Lippmann equation is strictly obeyed even at the smallest contact angles investigated ($\approx 5°$). Experimentally it is observed that the contact angle saturates above some material-dependent threshold voltage (see below). Within this range, the diverging fields at the contact line obviously induce effects that are not taken into account in equation (4), such as instabilities of the liquid surface (see below) or local dielectric breakdown of the insulating layers.

From a practical point of view, the conclusion from these calculations is that electrowetting can—on a macroscopic scale—indeed be treated as if it would simply change the surface energy. Deviations only play a role within a region of $\approx d_{\mathrm{ins}}$ of the contact line. In the experiments discussed below, we will focus on the global morphology of liquid microstructures. In this regime, electrowetting with patterned electrodes can be treated exactly the same way as conventional wetting of patterned substrates [9]. The equilibrium morphology is obtained by minimizing the free energy functional (equation (4)). In the majority of practical cases, the minimization has to be carried out numerically. One of the most frequently used and well-established tools to perform this minimization is the SURFACE EVOLVER [23]. This public domain software package calculates the shapes of free surfaces (represented by a triangulation grid) such that the F is minimal for a fixed liquid volume. Local contact angles on the surfaces have to be specified as boundary conditions for the minimization. Provided that gravitational effects can be neglected, the most important characteristic of any equilibrium liquid surface—in addition to satisfying Young's equation along the contact line—is that it has a constant mean curvature. These two requirements govern the mechanical equilibrium shape of fluid microstructures.

2. Experimental details

Reproducible electrowetting experiments require insulating layers with a variety of properties: the material should have a high dielectric strength. It should be stable and chemically inert when brought into contact with electrolyte solutions in order to prevent chemical reactions and irreversible adsorption of ions from the solution. Young's angle should be as large as possible in order to achieve a large contact angle tuning range. Finally, contact angle hysteresis should be small. For practical purposes, it is desirable to choose a material that can be prepared readily with standard laboratory equipment. One of the most widely used materials that satisfies all these criteria is amorphous Teflon AF®. This material can be either spin cast from solution or deposited by dip coating. Depending on the details of the deposition process (solution concentration and rotation frequency or dipping speed) films with a thickness ranging from a few tens of nanometres to a few micrometres can be prepared. Thicker films can be prepared by multiple dipping or spin coating, respectively. In order to improve the dielectric strength and to reduce the surface roughness, the samples are annealed in vacuum at 160 °C (between multiple deposition processes) and at 330 °C for approximately one hour at each temperature. For the experiments presented here, we used insulating layers with a thickness of 3–5 μm deposited in two dipping steps ($v_{\mathrm{dip}} = 1.7$ mm s^{-1}) from a 6 vol% solution of AF1601 in FC-75. The substrates were microscope slides covered by a transparent conductive layer of indium tin oxide (ITO). Sample preparation is performed inside a laminar flow cabinet. The dielectric strength of these layers scatters between 40 and 140 V μm^{-1}. The water contact angle on these surfaces is approximately 110°, with a hysteresis in air between 5° and 10°. In order to reduce the contact angle hysteresis, all the experiments presented here were performed in an oil environment (silicone oil; AK 5 from Wacker). Under these conditions, the contact angle hysteresis is reduced to 2°–3°. Furthermore, the contact angle at zero voltage increases to >160°. Presumably, this is due to a macroscopically thick oil film, which intervenes between the substrate and the liquid droplet. Another advantage of working under oil is the enlargement of the capillary length $\kappa = (\sigma_{\mathrm{lv}}/(g\Delta\rho))^{1/2}$, which allows for neglecting gravity up to droplet sizes of a few millimeters or even more in the case of perfect density matching (g is the gravitational acceleration and $\Delta\rho$ is the density difference between the liquid and the surrounding oil).

Operating liquids used in this study are mixtures of glycerol and solutions of NaCl in deionized water. Unless otherwise stated, salt concentrations (>1 mS cm^{-1}) are such that the

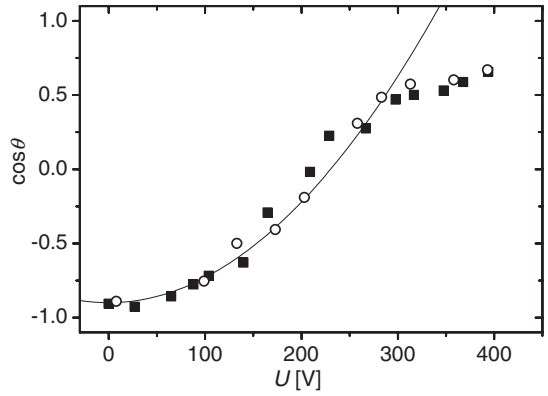

Figure 3. $\cos\theta$ versus U for advancing (filled squares) and receding (open circles) contact line in oil. Solid curve: parabolic fit.

liquid behaved as a perfect conductor. In order to reduce the possibility of permanent charge adsorption on the substrate surfaces, we used AC voltage ($U_{\text{eff}} = 0 \ldots 1$ kV) with a frequency of $\nu = 1 \ldots 10$ kHz. The morphology of the liquid was observed using a CCD camera with a zoom objective. In some cases, visibility and contrast were improved by adding fluorescent dye (fluorescein) to the liquid and by using appropriate filters for the excitation and detection of fluorescent light.

3. Results

3.1. Dependence on voltage, salt concentration, and frequency

In figures 1 and 3, we show a typical electrowetting setup and an electrowetting curve obtained under oil. The Lippmann equation is followed perfectly up to some critical voltage, approximately 300 V in the present example. Note that the deviation between increasing and decreasing voltage is negligible under these conditions. For the same type of sample in air, there appears both a hysteresis between increasing and decreasing voltage and there is difference between the first time the voltage is increased and subsequent cycles: after increasing and decreasing the voltage once, the original Young's angle is usually not recovered. Typically, we find a decrease in θ_{o} of 5°–10° in air.

Beyond the critical voltage, the contact angle becomes essentially independent of the applied voltage. This is the well-known contact angle saturation phenomenon that has been found in any electrowetting system studied so far. Despite a variety of explanations that have been proposed in the literature [24, 25], no general consensus on the origin of contact angle saturation has been reached so far. Most likely, several effects contribute to the phenomenon, with different effects dominating under different conditions. One particularly interesting effect is an instability of the contact line, as shown in figure 4. In this example, the droplet becomes unstable and emits small satellite droplets. This phenomenon was first observed by Berge *et al* [24]. The qualitative explanation is simple: from the theoretical discussion above, it is clear that the charge density at the contact line diverges. These equal charges repel each other. At small voltage, surface tension counteracts the electrostatic repulsion. Beyond some threshold voltage, however, electrostatic repulsion wins and the droplets begin to emit small charged droplets, as in classical Coulomb explosion in three dimensions. It is worth noting that we did not find any indication of such an instability in our two-dimensional numerical calculations (see above). This indicates that the instability is related to modulations of the contact line position, which depend on the full three-dimensional field distribution. Despite

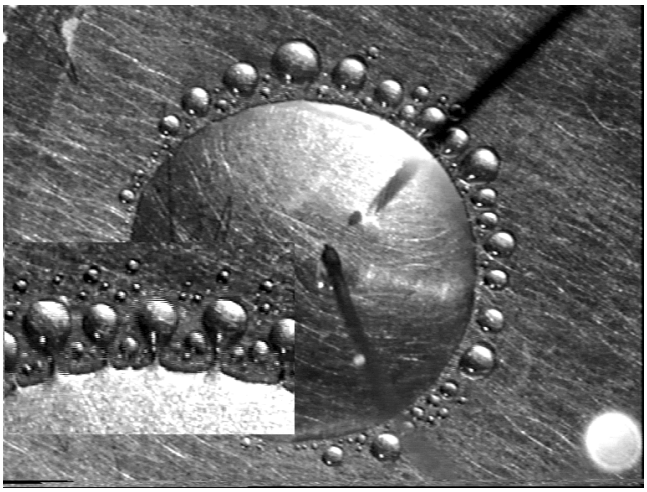

Figure 4. Contact line instability and emitted satellite droplets at high voltage (deionized water on silanized glass; droplet diameter ≈3 mm). Note the liquid necks between the satellites and the large droplet (inset).

the convincing qualitative picture, no quantitative model has been put forward so far to explain the instability.

Most interestingly, some of the satellite droplets are permanently connected to the reservoir via thin liquid channels.[4] These structures were found to be stable for several seconds although their Laplace pressure exceeds the one of the reservoir by up to three orders of magnitude. Similar to the field-induced surface distortions close to the contact line, we could show that the stabilization of these complex fluid microstructures is related to the Maxwell stress induced by the local electric field distribution. In this case, however, there is a potential drop along the liquid channel that connects the satellite droplet to the reservoir, which is crucial for the stabilization. The existence of these complex structures is thus related to the finite conductivity of the liquid [26].

Finite conductivity effects can also be demonstrated by monitoring contact angle variations at low voltage for poorly conductive liquids (see figure 5). Figure 3 was acquired with a salt concentration of 0.2 mol l^{-1} corresponding to a DC conductivity of ≈20 mS cm^{-1}. Under these conditions, the liquid behaves like a perfect conductor. In particular, this implies that the electrowetting curve is independent of both the AC frequency (provided that it is larger than the eigenfrequency of the droplet of ≈100 Hz) as well as the actual position of the electrode immersed into the droplet. From an applied point of view, it is important to explore the range of conductivity and frequency in which the perfect conductor model holds [27]. Figure 5 shows a liquid droplet with a conductivity of 3 μS cm^{-1} at constant voltage for the height h of the electrode above the substrate. Clearly, the contact angle increases the larger the distance between the electrode and the contact line. The reason is quite simple. The contact angle depends on the actual voltage at the contact line. For a poorly conductive liquid and a finite frequency of the applied voltage, there is a finite resistance between the electrode and the contact line. Simultaneously, the liquid at the contact line is capacitively coupled to the counter-electrode underneath the insulator. The resistance R and the capacitance C give rise to a geometry-dependent time constant $\tau = RC$.[5] If this relaxation time is larger than the

[4] The liquid in those experiments was a mixture of glycerol and deionized water [26].

[5] A similar situation was investigated by Shapiro *et al* [25], who calculated the field-distribution numerically.

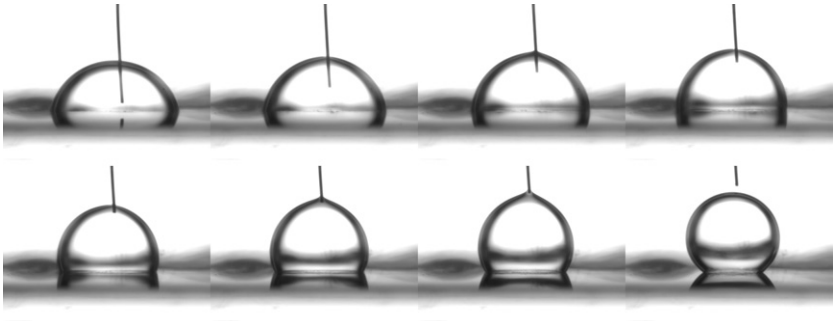

Figure 5. Geometry dependence of the droplet morphology for poorly a conductive liquid (deionized water; $\nu = 500$ Hz, $U = 67$ V, conductivity 3 μS cm^{-1}, wire–substrate-distance h: 0.2; 0.7; 1.1; 1.4; 1.7; 2.0; 2.3; 2.31 mm).

inverse of the applied AC frequency, the local voltage at the contact line will be smaller than the applied voltage. Hence the contact angle will be larger than expected on the basis of the applied voltage. By withdrawing the wire to some height h, we increase θ because R increases (figure 5). Similarly, we can keep the wire position constant and increase the frequency ν.

Figure 6 shows the contact angle versus electrode height h (a) and versus υ (b), respectively, for a variety of salt concentrations. Obviously, for the present millimeter-sized droplets the liquid can be considered as a perfect conductor for salt concentrations of 1850 μS cm^{-1} and above.

3.2. Stripe electrodes—planar substrates

In order to induce morphological changes other than transformations between spherical caps with different contact angle, we have to consider patterned electrodes. The simplest geometry consists of a stripe electrode, as sketched in figure 7(a). At zero voltage, droplets deposited on top of the stripe assume a spherical cap shape. As the voltage is increased, the contact angle on the stripe decreases following the Lippmann equation. As a consequence, the droplet is stretched along the stripe. Simultaneously, the maximum height a of the droplet decreases due to volume conservation (see top and side view images in figure 7(b)). In figure 7(c), we plot a/a_0, where a_0 is the height at zero voltage, as a function of the applied voltage. Most interestingly, a does not decrease continuously but displays a discontinuous transition at some volume-dependent threshold $U_{c,1}$. Above $U_{c,1}$, a becomes essentially independent of U: the morphology of the liquid corresponds to a segment of a cylinder, which is translationally invariant along the stripe—except for a cutoff due to the finite volume.

Upon decreasing the voltage, there is another discontinuous transition back to the stretched-droplet morphology at another threshold voltage $U_{c,2} < U_{c,1}$, and the original spherical cap shape is recovered at zero voltage. It is important to note that this morphological hysteresis loop is very reproducible; however, it appears only if the (normalized) liquid volume exceeds some critical value V_c. Below this threshold, the stretching of the droplet into a cylindrical morphology occurs in a continuous fashion (see the triangles in figure 7(c)). In fact, it was predicted by Brinkmann and Lipowsky [28] that a discontinuous morphological transition should occur in the present geometry. The morphology diagram that they derived is shown in figure 8. In the upper right, the liquid assumes the stretched-droplet morphology, whereas cylinder segments appear in the bottom left. The solid and dashed lines denote the stability limits of the stretched droplet and of the cylinder morphologies, respectively. In between the

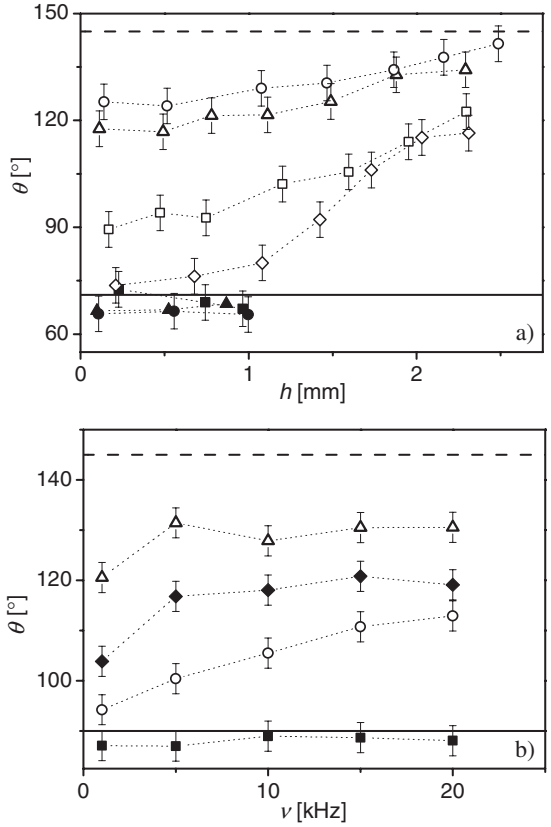

Figure 6. (a) Geometry dependence of θ (h: substrate–wire distance; $U = 67$ V) for various combinations of frequency and conductivity. Empty symbols: 3 μS cm^{-1} ($\nu = 500$ Hz: diamonds, $\nu = 1$ kHz: squares, $\nu = 5$ kHz: triangles, $\nu = 10$ kHz: circles); filled symbols: 18 mS cm^{-1}; same frequencies as above. (b) Contact angle θ versus frequency. Conductivity: 1850 μS cm^{-1} (squares), 197 μS cm^{-1} (circles), 91 μS cm^{-1} (diamonds), and 42 μS cm^{-1} (triangles). θ_o and $\theta(U)$ are shown as dashed and solid lines, respectively.

stability limits, both morphologies are at least metastable. That is, a given droplet can assume either morphology, depending on its history. The stability limits of both morphologies merge and end at a 'critical point' $(\tilde{V}_c, \theta_c) = (2.85, 39.2°)$. (Here, $\tilde{V} = V/b^3$ is the normalized droplet volume and b is the width of the stripe.) The data points in figure 8 refer to a series of experiments performed at various volumes slightly above and below the critical volume. Threshold contact angles for the transitions were determined by zooming to the contact line in side view images. Unfortunately, it was not possible to map out the morphological diagram at higher volumes because contact angle saturation sets in at around 30°. Given the slope of the solid line, this means that stretched droplets cannot be transformed into cylinders above $\tilde{V} \approx 5$. Within these limits, theoretical predictions regarding the occurrence of the transition and the presence of hysteresis, as well as the location of the critical point, are reproduced rather well. Note that there are no fitting parameters in this comparison.

Electrowetting thus allows for testing theoretical models of wetting on complex—in this case laterally structured—surfaces. Without a convenient external control parameter for tuning the wettability continuously, such a quantitative comparison is much more difficult to achieve

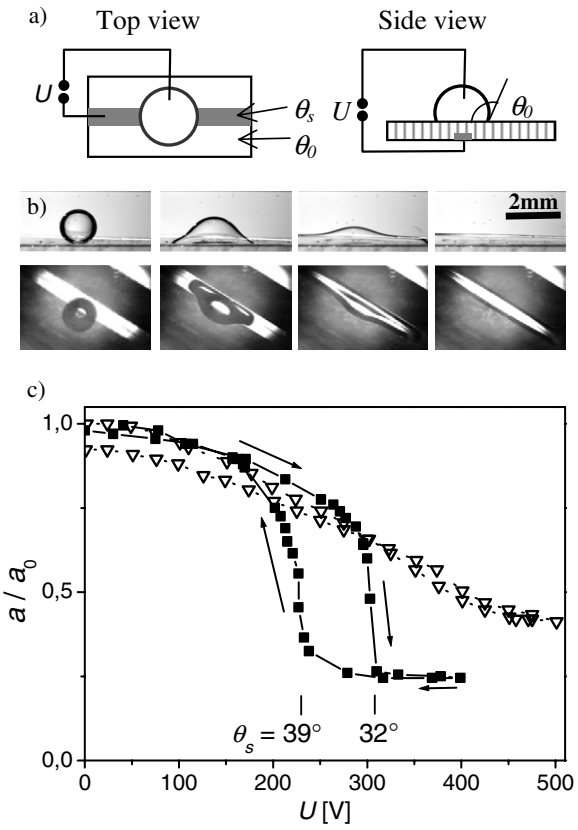

Figure 7. (a) Top and side views of a droplet on a substrate with stripe electrode (grey). $\theta = \theta_s(U)$ on the stripe; $\theta = \theta_o$ elsewhere. (The thickness of the insulating polymer (hatched) layer is not to scale.) (b) Video snapshots of morphological transition. ($\tilde{V} = 4.2$; voltage: 0, 250, 300, and 310 V, (left to right). Video clips can be viewed at www.wetting.de/electrowetting.htm). (c) Normalized droplet height versus voltage. Squares: $\tilde{V} = 4.2 > \tilde{V}_c$. Triangles: $\tilde{V} = 1.8 < \tilde{V}_c$.

because a whole series of substrates with different chemical but otherwise (roughness, contact angle hysteresis) identical properties would have to be prepared.

Additionally, the specific morphological transition described here may provide a useful pathway to a switch in a microfluidic device, as sketched in figure 9. By increasing and reducing the voltage on the stripe electrode, a connection between the two liquid reservoirs A and B can be established or broken, respectively. First experiments in that direction are very promising. They indicate, however, that the geometry of the electrodes has to be optimized. In particular, it seems necessary to prescribe a location on the stripe (e.g. by narrowing the electrode locally), where the cylinder is forced to rupture upon breaking the connection.

3.3. Stripe electrodes—parallel plate geometry

For various practical reasons, it is useful to consider a geometry with two substrates arranged in parallel plate geometry. For instance, this geometry allows for electrowetting without immersing electrodes directly into the liquid: the required voltage drop across the insulating layers can be achieved entirely by capacitive coupling. Furthermore, we demonstrated that

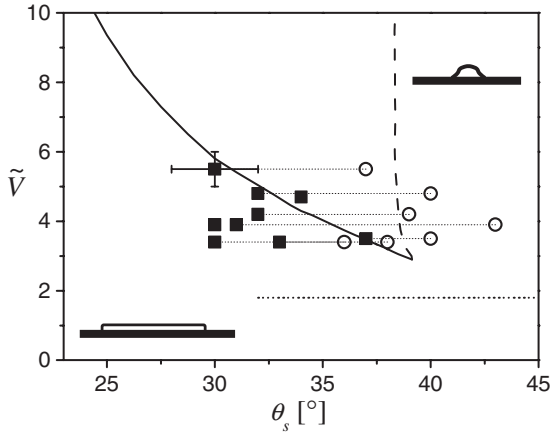

Figure 8. Morphological diagram (θ_s–$\tilde{V}$-plane). The solid and the dashed lines, which were taken from [28], represent numerically obtained instability lines for the bulge and channel morphologies, respectively. For small θ_s, only the channel (cylinder) state is stable; for high θ_s, only the bulge state is stable (cf sketched side view images of both morphologies). Between the solid and dashed lines both states are at least metastable. Solid squares and open circles represent the experimentally determined values for the bulge instability and channel instability, respectively. Thin dotted lines connect data points that were recorded in a single experimental run, as shown in figure 7(c). Typical error bars are as indicated for the upper left data point. For $\tilde{V} < \tilde{V}_c$ (thick dotted line), the morphological transition was continuous.

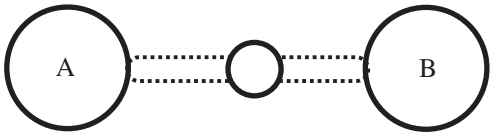

Figure 9. Sketch of a configuration that can be used to connect and separate two reservoirs A and B switching the central droplet reversibly into the cylinder configuration and back.

capillary bridges between two parallel electrowetting substrates with homogeneous electrodes can be induced to break and reform periodically in a self-excited fashion [29].

In the following, we will consider the case of one stripe electrode on each surface. The stripes can be aligned (figure 10) or mounted at an angle α (figure 13). In both cases, top view images of the liquid show a circular shape at zero voltage. As the voltage is increased, the contact angle on the stripes decreases and the droplets elongate progressively along the electrodes.

Let us first consider the case of parallel stripes ($\alpha = 0$). The upper and lower rows of figure 10 show a series of side and top view images, respectively, for increasing voltage. The viewing direction for the side view images was chosen perpendicular to the stripes. The images show zoomed views of the right edges of the droplet. The decrease in contact angle on the stripe as the voltage is increased is clearly seen. Simultaneously, top view images reveal changes in the projection of the droplet onto the substrate plane. Obviously, the boundary of the droplet is essentially parallel to the stripe for sufficiently high voltage.

Let us now analyse the morphological transformations in more detail. In figure 11, we plot the length of the droplet along the stripe as a function of the change in contact angle $\Delta \cos\theta$ for a series of different plate separations. Within the range of parameters studied here, the length is now a continuous function of $\Delta \cos\theta$ (i.e. of the applied voltage), independent of the

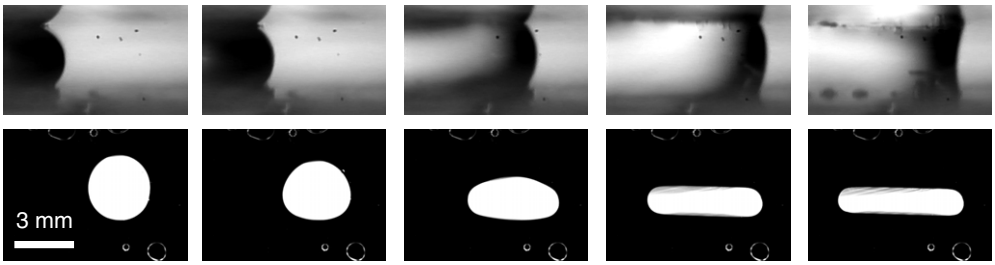

Figure 10. Typical side and top view snapshots for a droplet between parallel stripe electrodes for $U = 0$–400 V ($b = 1$ mm, $d = 330$ μm, $V = 2.2$ μl, $\nu = 10$ kHz). The aspect ratio of length and width increases from 1 to 5. (Top view images are fluorescence images.)

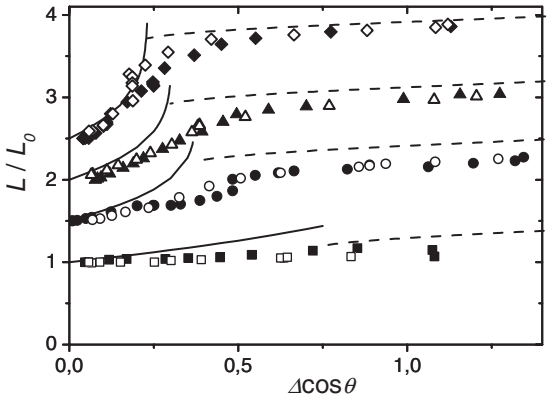

Figure 11. Comparison of droplet shape for experiment and analytic model ($V = 2.2$ μl, $b = 1$ mm, $\nu = 10$ kHz). Droplet length $L(\Delta\cos(\theta))$ (along the stripe) for $d = 830$ μm (squares), 400 μm (circles), 330 μm (triangles), and 250 μm (diamonds). Filled (open) symbols refer to increasing (decreasing) voltage. The data were shifted vertically for clarity. Solid and dashed curves show the analytical results for contact lines that are free or pinned at the stripe edge, respectively.

droplet volume. The discontinuous morphological transition that we found above for a single surface thus did not appear in the parallel plate geometry. Qualitatively, we attribute this to the fact that droplets in confined geometry have less freedom to adjust their morphology. Their configuration space is much more restricted, because of the fixed separation and fixed contact angles on the substrates.

3.4. Analytical model

The morphologies of liquid bridges between parallel perfectly non-wetting substrates with perfectly wetting stripes were investigated theoretically and numerically by Lipowsky and co-workers in several earlier papers [30]. Here, we are interested in variations of the liquid morphology as the wettability contrast is increased continuously from zero to a finite value. In order to describe the droplet elongation, we will make use of the requirement of constant mean curvature for liquid surfaces in mechanical equilibrium. As long as the in-plane dimensions L and B of the droplet (see figure 12) are large compared to the substrate separation d, the surface curvature in the plane perpendicular to the substrates is constant. That is, cross sections of the surfaces in the x–z- and in the y–z-planes are given by sections of circles. Their curvature is

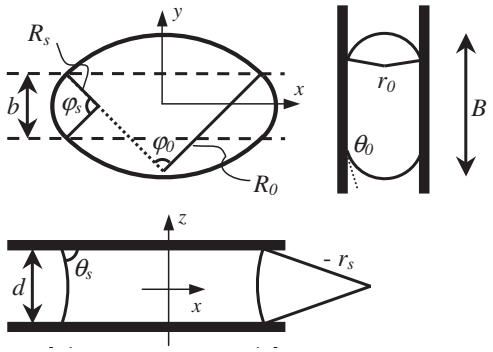

Figure 12. Top and side view sketches of the experimental setup. Two stripes of width b are at plate separation d. The droplet contour is composed of sections of circles with radius R_o, R_s, r_o and r_s in horizontal and vertical directions, respectively.

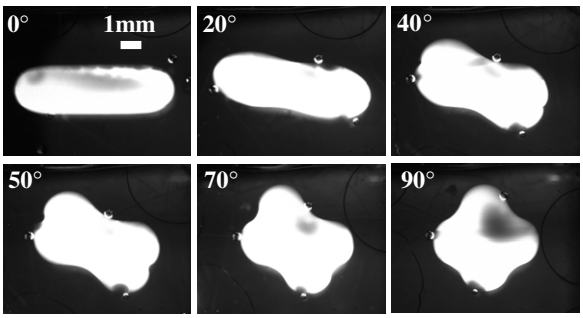

Figure 13. Top view of droplets between two parallel substrates with stripe electrodes for a variety of relative orientations from parallel (0°) to orthogonal (90°) ($U = 400$ V, $b = 2$ mm, $d = 640\,\mu$m, $\nu = 10$ kHz).

determined by the contact angle and by d:

$$\kappa_i = -2\cos(\theta_i)/d. \tag{8}$$

Here $i = s$ denotes the voltage-dependent contact angle and curvature on the stripe, whereas $i = 0$ denotes Young's angle and the corresponding curvature on the homogeneous part of the substrate. Note that κ_i changes sign when θ is switched from $\theta > 90°$ to $\theta < 90°$ or vice versa. In fact, we expect to find the same curvature κ_o or κ_s, respectively, in any plane containing the z-axis, except for a region of the order d around the edges of the stripes. For $d \ll b$ and for small droplet elongations (i.e. $L - B \ll L + B$), however, these regions are only a small fraction of the entire droplet surface. In order to approximate the global shape, we can thus assume that the (out-of-plane) curvature is κ_s everywhere on the stripe and κ_o everywhere outside. Given the requirement of constant mean curvature, this means that the in-plane curvatures $K_i = R_i^{-1}$ (see figure 12) must also assume constant values on both parts of the substrates. That is, the in-plane contour of the droplet is also given by segments of circles with radii R_s and R_o on the stripe and outside the stripes, respectively. In order to avoid kinks in the surface profiles, both segments have to join smoothly at the edges of the stripes. Since the values of κ_s and κ_o are determined by the geometry and the respective contact angles, R_s and R_o are the only unknown parameters in the model. Thus we need two equations in order to solve the problem. The first one is given by the requirement of constant mean curvature. The mean curvature of

the surface is given by the sum of κ_i and K_i.

$$\kappa_o + K_o = \kappa_s + K_s. \tag{9}$$

The second equation is the conservation of liquid volume. For $L, B \gg d$, it can be written as

$$V = A \cdot d = \text{constant} \tag{10}$$

where A is the area of the droplet within the plane parallel to the substrate. As far as volume conservation is concerned, the edges of the droplets are thus replaced by straight vertical surfaces. Using simple geometric formulae, A can be expressed as a function of the R_i and of the angles φ_i, as specified in figure 12.

$$A = R_s^2(\varphi_s - \sin\varphi_s) + R_o^2(\varphi_o - \sin\varphi_o) + 4R_sR_o \sin\frac{\varphi_s}{2}\sin\frac{\varphi_o}{2}. \tag{11}$$

For each value of the contact angle on the stripe, these equations have to be solved numerically for R_s and R_o, which can then be compared to the experimental results. Experimentally, it turns out that the length L of the droplet along the direction of the stripe can be quantified much more precisely. L can be expressed conveniently in terms of φ_s:

$$\frac{L}{b} = \frac{1-\cos(\varphi_s/2)}{\sin(\varphi_s/2)} + \frac{\cos(\varphi_s/2)}{\sin(\varphi_s/2) - \Delta\cos\theta \cdot b/d} \tag{12}$$

where φ_s depends on the numerically determined values of R_s and R_o.[6] Numerical solutions are plotted as solid curves in figure 11. The equation (12) predicts an increase in L up to a maximum value of[7]

$$L_{max} = V/(bd) + b(1 - \pi/4). \tag{13}$$

If $\Delta\cos\theta$ is increased further, L stays constant because of volume conservation. It is interesting to deduce the critical value $\Delta\cos\theta_c$ when L_{max} is reached. In order to do so, we note that R_o diverges as L approaches L_{max}. Simultaneously, $\varphi_s \to \pi$, which implies $R_s \to b/2$. If we insert this into equation (9), we find $\Delta\cos\theta_c = d/b$. It should be noted, however, that the model is expected to break down in this limit because major sections of the droplet surface approach the edges of the stripes. The present model thus cannot explain the continuous nature of the transition that was seen experimentally[8].

Obviously, the agreement between theory and experiment in figure 11 is quite satisfactory for small $\Delta\cos\theta$. In particular, the initial slope is nicely reproduced. Upon decreasing d, it increases dramatically. Upon approaching $\Delta\cos\theta_c$, however, the model breaks down, as expected, and underestimates the experimentally observed elongation. Beyond $\Delta\cos\theta_c$, the experimental data keep increasing, in contrast to the predictions of the model. This deviation is easy to rationalize. As $\Delta\cos\theta_c$ is approached, two assumptions of the two-dimensional model fail. First the contact angle along the arc with radius R_o is no longer equal to Young's angle. For $R_o \to \infty$, the contact line is pinned along the edge of the stripe. Hence the local pinned contact angle θ_p can adopt any value $\theta_o > \theta_p > \theta_s$. As $\Delta\cos\theta$ is increased beyond $\Delta\cos\theta_c$, θ begins to decrease along the pinned sections of the contact line. During this process, liquid that was originally protruding slightly beyond the edges of the stripe is pushed inward. Due to volume conservation this leads to an increase of L even for $L > L_{max}$. As mentioned above

[6] A similar expression can be given for the width B of the droplet perpendicular to the stripe: $B/b = (1 - \Delta\cos\theta b/d)/(\sin(\varphi_s/2) - \Delta\cos\theta b/d)$.

[7] In order to obtain the analytic expression for L_{max}, equation (11) must to be expanded asymptotically for $\phi_s \to \pi$ and $\Delta\cos\theta \to d/b$ simultaneously.

[8] Numerical studies of liquid bridges between perfectly wetting stripes also suggest that the elongation should be continuous [31].

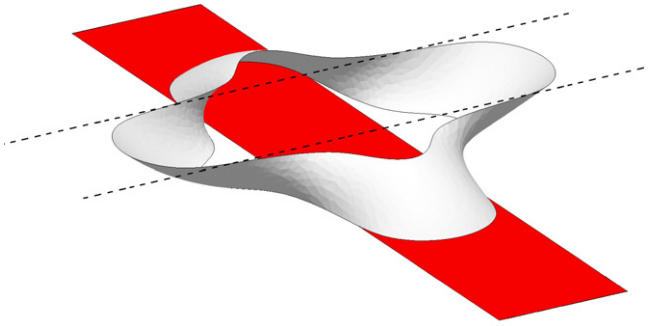

Figure 14. Numerically computed three-dimensional view of a liquid droplet between crossed hydrophilic stripes by surface evolver ($\alpha = 90°$).

(see equation (10)), the contribution of this part to the total liquid volume is not taken into account within the model.

In fact the elongation in the pinned state can also be modelled rather easily. For geometric reasons, we have $R_o = \infty$ and $R_s = b/2$. If we include the previously neglected contribution, the length of the droplet along the stripe is given by

$$L = \frac{\frac{V}{bd} + b(1 - \frac{\pi}{4} + \frac{2A(\theta_p)}{bd})}{1 + \frac{2A(\theta_p)}{bd}} \tag{14}$$

where $A(\theta_p) = d^2[2\theta_p - \pi - \sin(\theta_p - \pi)]/8\sin^2(\theta_p - \pi/2)$ is the area of the previously neglected volume (see figure 12). If we use $\cos(\theta_p) = \cos(\theta_s) - d/b$ from equation (9) we obtain L as a function of θ_s. The dashed curves in figure 11 show the result for $\Delta\cos\theta > \Delta\cos\theta_c$. The discontinuity between the two models at $\Delta\cos\theta = \Delta\cos\theta_c$ arises from the different relation between L and V: for $\Delta\cos\theta = \Delta\cos\theta_c$, $\theta_p > 90°$ in the present case. Therefore the cross-sectional area of the droplet is larger in the second model than in the first. Hence L must be shorter.

Again, one may apply this voltage-induced droplet elongation in order to establish and break a connection between two reservoirs (cf figure 9), but now in a parallel plate geometry. Experiments in that direction are currently under way in our laboratory.

Let us now consider the case of rotated stripes ($\alpha \neq 0$). Figure 13 shows a series of top view images as α is increased from 0° to 90° at constant voltage. At $\alpha = 90°$, the top view images have a four-fold symmetry. It should be noted, however, that this is due to the projection of the actual liquid morphology onto the substrate plane. In reality, the three-dimensional droplet is elongated along the directions of the stripes on the top and bottom surface, respectively. Figure 14 shows a three-dimensional view of the equilibrium morphology of such a droplet at $\alpha = 90°$. The surface was calculated numerically using the SURFACE EVOLVER with boundary conditions on the surface and on the stripe as extracted from the experiments. Figure 15 shows a comparison between experimental top and side views and equilibrium profiles as extracted from the numerical calculations for two different plate separations d. The quantitative agreement illustrates that numerical calculations are very reliable in describing liquid morphologies on patterned substrates.

4. Discussion and conclusion

The experiments described above provide a solid basis for the development of electrowetting-based open microfluidic systems. It was shown that electrowetting could be thought of simply as a tool to control the contact angle of conductive liquids. With respect to the equilibrium morphology, differences between chemically and electrically induced variations of the contact

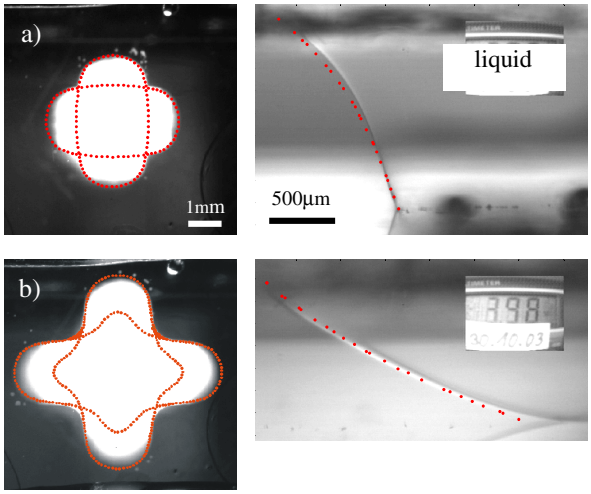

Figure 15. Liquid shape in crossed geometry ($U = 400$ V, $b = 2$ mm, $V = 12$ μl, $\nu = 10$ kHz). The plate separation is (a) $d = 1430$ μm and (b) $d = 640$ μm. Experimental top and side views are shown together with overlaid dotted lines taken from numerical calculations.

angle are negligible except for a small region close to the contact line. Restrictions with respect to conductivity are not very stringent. For a conductivity of 1 mS cm^{-1} and above, as typically encountered for biological buffer solutions, liquids behave as perfect conductors up to a few tens of kilohertz.

In combination with suitable electrode patterns, the morphology of fluid microstructures may be tuned electrically. These morphological changes may occur as discontinuous morphological transitions, as in the case of droplets on top of a stripe electrode on a single surface, or they may occur as continuous transformations as in the case of two opposing surfaces with parallel stripe electrodes. In some cases, the transformations can be described using simple analytical models, which reproduce almost quantitatively the experimentally observed behaviour. In this situation, the models can be used as design tools for the optimization of devices that perform more complex fluid handling tasks such as a switching on and off a connection between two reservoirs. In the case of more complex geometries, the description of the equilibrium structure relies on numerical tools such as the SURFACE EVOLVER. On a length scale of several hundred nanometres and above, these tools were proven to work reliably and can thus be used for design purposes in the future.

Wetting on chemically patterned substrates is by now rather well understood. The same conclusion applies for electrowetting with patterned electrodes, except for a few open issues related to the behaviour at high voltage, namely contact angle saturation and contact line instabilities. Future trends will probably address more applied issues like the realization of complex microfluidic systems. This will include combinations of patterned electrodes with chemical patterns on the surface in order to obtain more complex functionality. Another issue that remains to be understood is the connection between electrowetting and flow in fluid microstructures. In this case, electrokinetic effects may induce a behaviour that is substantially different to dynamic wetting on chemically patterned substrates.

Acknowledgments

We would like to thank Martin Brinkmann for fruitful discussions and for advice regarding numerical procedures. We are indebted to Renate Nikopoulos for assistance during the experiments and with sample preparation. This work was supported by the German Science Foundation within the priority program ‘Wetting and Structure Formation at Interfaces’.

References

[1] Lipowsky R 2001 *Curr. Opin. Colloid Interface Sci.* **6** 40
Lenz P and Lipowsky R 1998 *Phys. Rev. Lett.* **80** 1920
Schäfle C, Bechinger C, Rinn B, David C and Leiderer P 1999 *Phys. Rev. Lett.* **83** 5302
Herminghaus S, Gau H and Mönch W 1999 *Adv. Mater.* **11** 1393
Darhuber A A, Troian S M, Miller S M and Wagner S 2000 *J. Appl. Phys.* **87** 7768
Rascon C and Parry A 2000 *Nature* **407** 986
Bico J, Tordeux C and Quéré D 2001 *Europhys. Lett.* **55** 214
Lafuma A and Quéré D 2003 *Nat. Mater.* **2** 457
[2] Gau H, Herminghaus S, Lenz P and Lipowsky R 1999 *Science* **283** 46
[3] Kataoka D W and Troian S M 1999 *Nature* **402** 794
[4] Bauer C and Dietrich S 1999 *Phys. Rev.* E **60** 6919
[5] Ulman A 1991 *An Introduction to Ultrathin Organic Films: From Langmuir-Blodgett to Self-Assembly* (Boston, MA: Academic)
[6] Xia Y and Whitesides G M 1998 *Angew. Chem. Int. Edn Engl.* **37** 550
[7] Herminghaus S, Fery A and Reim D 1997 *Ultramicroscopy* **69** 211
Pompe T, Fery A and Herminghaus S 1998 *Langmuir* **14** 2585
Fery A, Pompe T and Herminghaus S 1999 *J. Adhes. Sci. Technol.* **13** 1071
[8] Pompe T and Herminghaus S 2000 *Phys. Rev. Lett.* **85** 1930
Mugele F, Becker T, Nikopoulos R, Kohonen M and Herminghaus S 2002 *J. Adhes. Sci. Technol.* **16** 951
Checco A, Guenoun P and Daillant J 2003 *Phys. Rev. Lett.* **91** 186101
[9] Lenz P, Bechinger C, Schäfle C, Leiderer P and Lipowsky R 2001 *Langmuir* **17** 7814
[10] Whitesides G M and Stroock A D 2001 *Phys. Today* **54** 42
Pfohl T *et al* 2003 *Chem. Phys. Chem.* **4** 1291
[11] Darhuber A A, Valentino J P, Davis J M and Troian S M 2003 *Appl. Phys. Lett.* **82** 657
Garnier N, Grigoriev R O and Schatz M F 2003 *Phys. Rev. Lett.* **91** 054501
[12] Ichimura K, Oh S-K and Nakagawa M 2000 *Science* **288** 1624
[13] Huber D L, Manginell R P, Samara M A, Kim B I and Bunker B C 2003 *Science* **301** 352
[14] Lahann J, Mitragotri S, Tran T-N, Kaido H, Sundaram J, Choi I S, Hoffer S, Somorjai G A and Langer R 2003 *Science* **299** 371
Gallardo B S, Gupta V K, Eagerton F D, Jong L I, Craig V S, Shah R R and Abbott N L 1999 *Science* **283** 57
[15] Quilliet C and Berge B 2001 *Curr. Opin. Colloid Interface Sci.* **6** 1
[16] Berge B and Peseux J 2000 *Eur. Phys. J.* E **3** 159
Krupenkin T, Yang S and Mach P 2003 *Appl. Phys. Lett.* **82** 316
[17] Acharya B R, Krupenkin T, Ramachandran S, Wang Z, Huang C C and Rogers J A 2003 *Appl. Phys. Lett.* **83** 4912
[18] Hayes R A and Feenstra B J 2003 *Nature* **425** 383
[19] Landau L D and Lifschitz E M 1985 *Theoretische Physik* vol 8 *Elektrodynamik der Kontinua* (Berlin: Akademie)
[20] deGennes P G 1985 *Rev. Mod. Phys.* **57** 827
[21] Buehrle J, Herminghaus S and Mugele F 2003 *Phys. Rev. Lett.* **91** 086101
[22] Finn R 1986 *Equilibrium Capillary Surfaces* (New York: Springer)
[23] Brakke K 1992 *Exp. Math.* **1** 141
[24] Vallet M, Vallade M and Berge B 1999 *Eur. Phys. J.* B **11** 583
[25] Peykov V, Quinn A and Ralston J 2000 *Colloid. Polym. Sci.* **278** 789
Verheijen H J J and Prins M W J 1999 *Langmuir* **15** 6616
Shapiro B, Moon H, Garrell R L and Kim C-J 2003 *J. Appl. Phys.* **93** 5794
Kang K H 2002 *Langmuir* **18** 10318
[26] Mugele F and Herminghaus S 2002 *Appl. Phys. Lett.* **81** 2303
[27] Jones T B *et al* 2003 *Langmuir* **19** 7646
Jones T B 2002 *Langmuir* **18** 4437
[28] Brinkmann M and Lipowsky R 2002 *J. Appl. Phys.* **92** 4296
[29] Klingner A, Herminghaus S and Mugele F 2003 *Appl. Phys. Lett.* **82** 4187
[30] Swain P S and Lipowsky R 2000 *Europhys. Lett.* **49** 203
Valencia A, Brinkmann M and Lipowsky R 2001 *Langmuir* **17** 3390
[31] Brinkmann M 2002 *PhD Thesis* University of Potsdam, Germany